The Astrophysical Journal, 804:54 (8pp), 2015 May 1 doi:10.1088/0004-637X/804/1/54

ON THE FUNCTIONAL FORM OF THE UNIVERSAL STAR-FORMATION LAW

Andrés Escala
Departamento de Astronomía, Universidad de Chile, Casilla 36-D, Santiago, Chile; aescala@das.uchile.cl
Received 2014 November 30; accepted 2015 February 13; published 2015 April 30

ABSTRACT

We study the functional form of the star-formation law using the Vaschy–Buckingham Pi theorem. We find that it should have the form $\dot{\Sigma}_\star \propto \sqrt{\frac{G}{L}}\,\Sigma_{\rm gas}^{3/2}$, where L is a characteristic length that is related to an integration scale. With a reasonable estimate for L, we find that galaxies of different types and redshifts, including low-surface-brightness galaxies and individual star-forming regions in our Galaxy, obey this single star-formation law. We also find that, depending on the assumption for L, this star-formation law adopts different formulations of $\dot{\Sigma}_\star$ scaling that are widely studied in the literature: $\Sigma_{\rm gas}^{3/2}$, $\Sigma_{\rm gas}/t_{\rm orb}$, $\Sigma_{\rm gas}/t_{\rm ff}$ and $\Sigma_{\rm gas}^{2}/v_{\rm turb}$. We also study secondary controlling parameters of the star-formation law based on the current evidence from numerical simulations, and we find that for galaxies the star-formation efficiency should be controlled, at least, by the turbulent Toomre parameter and the sonic and Alfvénic Mach numbers.

Key words: galaxies: formation – stars: formation – stars: general

1. INTRODUCTION

Galaxies are building blocks of the universe, and the galaxies themselves are constituted by stars. Therefore, understanding the rate at which galaxies form their stars is a fundamental part of understanding how the universe evolves. For that reason, there has been considerable effort to understand the rate at which galaxies fill the cosmos with stars.

Observations of normal spiral galaxies by Schmidt (1959) originally suggested that their star-formation rates (SFRs) scale with their gas content. This was extended to galaxies with higher SFR by Kennicutt (1998), leading to an empirical law for star formation called the Kennicutt–Schmidt (KS) law: $\dot{\Sigma}_{\rm star} = \epsilon_{\rm SF}\Sigma_{\rm gas}^{1.4}$, where $\Sigma_{\rm gas}$ and $\dot{\Sigma}_{\rm star}$ are the gas surface density and SFR per unit area. However, Bigiel et al. (2008), Leroy et al. (2008), Wyder et al. (2009), and Shi et al. (2011) found deviations from the ∼1.4 slope at lower surface densities. In addition, Daddi & Elbaz et al. (2010b) and Genzel et al. (2010) studied this relation for high-redshift galaxies, Shi et al. (2014) the effects of metallicity on the SFR, and Guillard et al. (2014) the role of radio jets, all finding possible departures from a single law. Also, for major mergers, Xu et al. (2014) and Hodge et al. (2015) found higher SFRs for spatially resolved individual regions.

On the theoretical side, considerable literature has focused on analytic calculations with a considerable level of assumptions and free parameters, thus, it is hard to test their validity against the observed data (Krumholz & McKee 2005; Krumholz et al. 2012; Hopkins 2013, just to mention a few attempts). Moreover, several galactic-scale numerical simulations (Li et al. 2005; Stinson et al. 2006; Tasker & Bryan 2006; Tasker & Tan 2009; Becerra & Escala 2014), using completely different thermal physics, accuracy of hydrodynamic method, star formation/feedback prescriptions, and so on, are all able to find an SFR in agreement with the KS law, regardless of the different physics implemented.

In this paper we propose a different approach: using the Vaschy–Buckingham theorem to guide an analysis of the current observational and numerical evidence on the subject to see what we can learn from them and if it is possible to infer functional forms and controlling parameters of the universal star-formation law. Our goal is to summarize the current evidence into a unique physical equation valid at all scales, in which variations of its physical variables explain the variations of the observed SFRs, from individual clouds in the Milky Way to galaxies in the early universe.

This work is organized as follows. We start with a dimensional analysis of the star-formation law in order to find a physical relation in agreement with the current observational and numerical evidence in Section 2. Section 3 continues with a discussion on the characteristic length introduced in Section 2, and tests candidates against the SFRs in galaxies of different types and redshifts. In Section 4 we study the physics that determines this characteristic length, deriving several formulations for the star-formation law that appears in the literature. Finally, in Section 5 we discuss the results of this work.

2. DIMENSIONAL ANALYSIS OF THE STAR-FORMATION LAW

The Vaschy–Buckingham Pi theorem defines the rules to be fulfilled by any meaningful physical relation, and it is a formalization of Rayleigh's method of dimensional analysis. The theorem states that if there is a physically meaningful equation involving a certain number, n, of physical variables and k is the number of relevant dimensions, then the original expression is equivalent to an equation involving a set of $p = n - k$ dimensionless parameters constructed from the original variables. Mathematically speaking, if we have the physical equation

$$F(A_1, A_2, \ldots, A_n) = 0, \tag{1}$$

where the A_i are the n physical variables that are expressed in terms of k independent physical units, Equation (1) can be written as

$$f(\Pi_1, \Pi_2, \ldots, \Pi_{n-k}) = 0, \tag{2}$$

where the $\Pi_{\rm i}$ are dimensionless parameters constructed from the $A_{\rm i}$ by $p = n - k$ dimensionless equations of the form $\Pi_{\rm i} = A_1^{\rm m_1}A_2^{\rm m_2}\cdots A_{\rm n}^{\rm m_n}$. We will use this theorem to design a physically meaningful equation for the universal star-formation law.

In the process of finding the functional form of any physical equation through dimensional analysis, it is critical to choose the relevant physical variables. We will perform this iteratively for the universal star-formation law. Because this problem has a minimum of three relevant dimensions, mass $[M]$, length $[L]$, and time $[T]$, we need at least four physical variables in order to have one dimensionless parameter Π_1. Motivated by the KS law, $\dot{\Sigma}_\star$ and $\Sigma_{\rm gas}$ must be the first two physical variables. There is little doubt that gravity plays a critical role in the star-formation problem, ever since the early analytical results by Jeans (1902), Bonnor (1956), and Ebert (1955) and the numerical work by Larson (1969) and Penston (1969). Therefore, G should appear somewhere in any star-formation law and is our third choice. For our final fourth physical variable, either a characteristic time or length could work; -however, to avoid the trivial dependence proportional to $\Sigma_{\rm gas}/\tau$ (e.g., Silk 1997, Elmegreen 1997), we choose to use a characteristic length that we call L.

Finding the first dimensionless parameter is straightforward by looking at integer exponents such as $\Pi_1 = G^{a_1}\Sigma_{\rm gas}^{b_1}L^{c_1}\dot{\Sigma}_\star$ have no dimensions. This is equivalent to force $[L]^{3a_1-2b_1+c_1-2}$, $[M]^{-a_1+b_1+1}$, $[T]^{-2a_1-1}$ being dimensionless, which has the unique solutions $a_1 = -1/2$, $b_1 = -3/2$, and $c_1 = 1/2$. This implies that the dimensionless parameter is $\Pi_1 = G^{-1/2}\Sigma_{\rm gas}^{-3/2}L^{1/2}\dot{\Sigma}_\star$, and if the star-formation law depends only on these four physical variables, the Vaschy–Buckingham Pi theorem states that it should be a function f such that $f(\Pi_1 = G^{-1/2}\Sigma_{\rm gas}^{-3/2}L^{1/2}\dot{\Sigma}_\star) = 0$. Additionally, if f has a zero that we call ϵ, such that $f(\epsilon) = 0$, this implies that

$$\dot{\Sigma}_\star = \epsilon\sqrt{\frac{G}{L}}\,\Sigma_{\rm gas}^{3/2}, \tag{3}$$

which has a dependence on surface density quite similar to the standard formulation for the star-formation law, but it has an extra term L. If such characteristic length is constant, we recover the KS law with almost the observed slope ($n \sim 1.4$; Kennicutt 1998). In summary, the Vaschy–Buckingham Pi theorem is telling us that the standard formulation of the star-formation law needs to be at least corrected by a characteristic length in order to have the proper dimensions.

In addition to this length correction, other physical variables should have a role in controlling the rate at which galaxies form their stars in the universe. We will explore a few possibilities subsequently.

2.1. Role of Turbulence

At intermediate, giant molecular cloud (GMC) scales, it is commonly believed that turbulence governs the GMC dynamics, with typical thermal Mach numbers ($\mathcal{M}_{\rm s} = v_{\rm turb}/C_{\rm S}$) of the order 10–20 (Mac Low & Klessen 2004). Moreover, it has been suggested by Larson (1979, 1981) and others (see for example Ballesteros-Paredes et al. 2007 and references therein) that the structure and dynamics of the interstellar matter (ISM) on these intermediate scales is roughly self-similar and described by power laws, as in a turbulent cascade.

In order to explore if the three-dimensional rms velocity of turbulent motions, $v_{\rm turb}$, is a fifth physical variable in the star-formation law, a Π_2 should be constructed because the Vaschy–Buckingham Pi theorem now allows $5 - 3 = 2$ dimensionless parameters. The parameter $\Pi_2 = v_{\rm turb}G^{a_2}\Sigma_{\rm gas}^{b_2}L^{c_2}$ has no dimensions for a unique solution of $a_2 = -1/2$, $b_2 = -1/2$, and $c_2 = -1/2$, implying a second dimensionless parameter $v_{\rm turb}G^{-1/2}\Sigma_{\rm gas}^{-1/2}L^{-1/2}$. In this case, the Pi theorem states that there is an equation $f(\Pi_1, \Pi_2) = 0$, and if f is regular and differentiable, we can use the implicit function theorem to advocate for the existence of a function $\Pi_1 = \epsilon(\Pi_2)$. This implies that if the turbulent rms velocity is an additional physical variable in the star-formation law, Equation (3) should be replaced by

$$\dot{\Sigma}_\star = \epsilon\left[\frac{v_{\rm turb}}{\sqrt{G\Sigma_{\rm gas}L}}\right]\sqrt{\frac{G}{L}}\,\Sigma_{\rm gas}^{3/2}, \tag{4}$$

where ϵ is now a function of $v_{\rm turb}\left(G\Sigma_{\rm gas}L\right)^{-1/2}$, a parameter that quantifies the relative strength of turbulence and gravity.

The dependence of ϵ on the second dimensionless parameter Π_2 can be directly compared against numerical experiments that study fragmentation in turbulent GMCs. Padoan et al. (2012) found that the SFR per free-fall time, $\epsilon_{\rm ff}$, strongly depends on the free-fall time per turbulent crossing time. The turbulent crossing time is defined by Padoan et al. (2012) as $t_{\rm dyn} = L/2v_{\rm turb}$ and the free-fall time as $t_{\rm ff} = \left(3\pi/32G\rho_0\right)^{1/2}$, where ρ_0 is the mean density. For $\rho_0 = \Sigma_{\rm gas}/L$, it is straightforward to find that their Equation (1) is equivalent to our Equation (4), in particular that $\epsilon_{\rm ff}$ has the same dimensionless dependence as $\epsilon(\Pi_2)$ within geometrical factors ($t_{\rm ff}/t_{\rm dyn} = (3\pi/8)^{1/2}v_{\rm turb}\left(G\Sigma_{\rm gas}L\right)^{-1/2}$).

Using the Pi theorem, we also found the main dependence suggested by state-of-the-art simulations of turbulent fragmentation because this dimensionless parameter Π_2 is also equivalent to the virial parameter, $\alpha_{\rm virial} = 2T/W$, used in previous works (Padoan & Nordlund 2011). Padoan et al. (2012) quantified this strong dependence by the fitting formula $\epsilon_{\rm ff} \propto \exp(-1.6t_{\rm ff}/t_{\rm dyn})$, which is equivalent to $\epsilon_{\rm ff} \propto \exp(-1.74v_{\rm turb}\left(G\Sigma_{\rm gas}L\right)^{-1/2})$.

2.2. Small-scale Physics: Role of Thermal Pressure and Magnetic Fields

There is little doubt that the final barrier that the self-gravity of interstellar gas should overcome to form a star is thermal pressure. In addition, magnetic fields are often advocated as a relevant source of support (Mouschovias 1974, Shu 1997). We will start by analyzing the role of thermal pressure because this is what eventually stops the collapse at stellar densities.

To include the thermal sound speed, $C_{\rm S}$, as the sixth physical variable in the star-formation law, a Π_3 should be constructed. The parameter $\Pi_3 = C_{\rm S}G^{a_3}\Sigma_{\rm gas}^{b_3}L^{c_3}v_{\rm turb}^{d_3}$ has no dimensions for two possible solutions: (1) $a_3 = b_3 = c_3 = 0$, $d_3 = -1$ and (2) $a_3 = b_3 = c_3 = -1/2$, $d_3 = 0$. We will focus on case (1), $\Pi_3 = C_{\rm S}/v_{\rm turb}$, because there is numerical work that studies the role of the sonic Mach number $\mathcal{M}_{\rm s} = v_{\rm turb}/C_{\rm S}$.

Using MHD simulations, covering a substantial range of observed cloud parameters with Mach numbers $\mathcal{M}_{\rm s} = v_{\rm turb}/C_{\rm S} = 5 - 50$, Federrath (2013) found that the observed scatter in the star-formation law can be primarily explained by physical variations in the turbulent Mach number $\mathcal{M}_{\rm s}$. This work also found that magnetic fields reduce the star-formation efficiency, ϵ, but only very marginally.

To include magnetic fields in our analysis, it is easier to use the Alfvénic velocity, v_a, in order to compare their

strength relative to thermal pressure. A $\Pi_4 = v_a G^{a_4} \Sigma_{\rm gas}^{b_4} L^{c_4} v_{\rm turb}^{d_4}$ should be constructed that has again no dimensions for two possible solutions: (1) $a_4 = b_4 = c_4 = 0$, $d_4 = -1$ and (2) $a_4 = b_4 = c_4 = -1/2$, $d_4 = 0$. For the first case, $\Pi_4 = v_a / v_{\rm turb} = \mathcal{M}_a^{-1}$ is the inverse of the Alfvénic Mach number.

Padoan et al. (2012) found that the star-formation efficiency, ϵ, has a complex but weak dependence on $\mathcal{M}_a$, varying by less than a factor of two for characteristic values of $\mathcal{M}_a$. However, this work found that ϵ is insensitive to variations of $\mathcal{M}_{\rm s}$. This disagreement with Federrath (2013) might be due to the dynamical range studied: $\mathcal{M}_{\rm s} = 10 - 20$ in Padoan et al. (2012), compared to $\mathcal{M}_{\rm s} = 5 - 50$ in Federrath (2013). The range $\mathcal{M}_{\rm s} = 10 - 20$ might be justified for local GMCs, but for extragalactic sources such as starbursts or high-z galaxies, a range like the one in Federrath (2013) is better justified.

Including thermal pressure and magnetic fields, the Pi theorem states that there is an equation $f(\Pi_1, \Pi_2, \Pi_3, \Pi_4) = 0$, and if f is regular and differentiable, the implicit function theorem guarantees the existence of a function $\Pi_1 = \epsilon(\Pi_2, \Pi_3, \Pi_4)$. The latter is equivalent to a star-formation law of the form

$$\dot{\Sigma}_\star = \epsilon\left[\frac{v_{\rm turb}}{\sqrt{G\Sigma_{\rm gas} L}}, \mathcal{M}_{\rm s}, \mathcal{M}_a\right]\sqrt{\frac{G}{L}}\,\Sigma_{\rm gas}^{3/2}. \quad (5)$$

The options (2) for Π_3 and Π_4 are respectively $C_{\rm S}\left(G\Sigma_{\rm gas} L\right)^{-1/2}$ and $v_a\left(G\Sigma_{\rm gas} L\right)^{-1/2}$. These options are equivalent to $\Pi_3 = \Pi_2/\mathcal{M}_{\rm s}$ and $\Pi_4 = \Pi_2/\mathcal{M}_a$, a combination of the previous dimensionless parameters.

We can continue with this iterative process of searching for physical variables by including other controlling parameters suggested in the literature, such as the molecular mass fraction f_{H_2} (Krumholz & McKee 2005) or the metallicity (Dib et al. 2011; Shi et al. 2014). However, we prefer to focus in this paper on the dynamical variables just mentioned, which are motivated by both observational and numerical studies.

3. ON THE CHARACTERISTIC LENGTH L

We have been able to find a star-formation law that, in addition to being dimensionally correct, has several dependencies in agreement with both the KS law (for a constant characteristic length L) and numerical experiments that study star formation within GMCs. However, thus far the characteristic length L is a free parameter without any physical interpretation.

We will start with the simplest possible choice for characteristic length L, the region total radius R, which is a natural scale of galaxies and star-forming regions, and later evolve to more sophisticated choices. Because the goal is to find a universal law valid at all scales, we include data from individual star-forming clouds, up to extended galaxies like low-surface-brightness (LSB) galaxies (five orders of magnitude variations in R). We also include normal spiral, local starburst, and high-redshift galaxies.

In the large dynamical range studied, which needs to be displayed on a log–log plot, the relation is dominated by order of magnitude variations of the primary dependencies. For that reason, Π_1 will dominate over the other dependencies, so for simplicity we will assume that $\epsilon(\Pi_2, \Pi_3, \Pi_4) = \epsilon$ is constant in this section (Equation (3)).

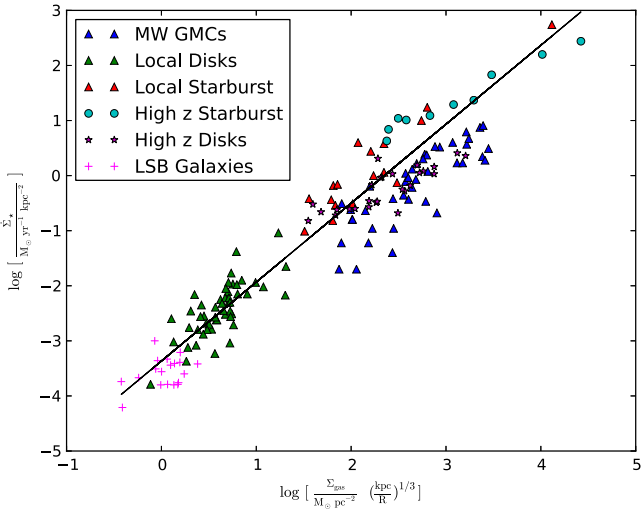

Figure 1. SFR density as a function of the gas surface density, divided by the one-third power of the radius. The symbols are as follows: blue triangles are galactic GMCs taken from Lada et al. (2010) and Heiderman et al. (2010); green and red triangles are local spiral galaxies and ultra-luminous infra-red galaxies (ULIRGs) from Kennicutt (1998); purple stars and cyan filled circles are high-z disks (Daddi et al. 2010a; Tacconi et al. 2010) and starburst galaxies (Genzel et al. 2010); and pink crosses are LSB galaxies from Wyder et al. (2009).

Figure 1 shows the SFR per unit area against $\Sigma_{\rm gas} R^{-1/3}$, with R the radius of each galaxy or star-forming region. The gas surface density $\Sigma_{\rm gas}$ and SFR per unit area $\dot{\Sigma}_\star$ for each data point were taken for LSB galaxies (Wyder et al. 2009), normal spirals or local starbursts (Kennicutt 1998), high-redshift disks (Daddi et al. 2010a; Tacconi et al. 2010), high-redshift starbursts (Genzel et al. 2010), and galactic GMCs (Lada et al. 2010; Heiderman et al. 2010). In addition to the previous references, for the radius R, data was taken from Young et al. (1995) for normal spirals, Smith & Harvey (1996), Downes & Solomon (1998), Kenney et al. (1992), Wild et al. (1992), and Telesco et al. (1993) for local starbursts, Genzel et al. (2010) for high-redshift disks, and Krumholz et al. (2012) for galactic GMCs.

All galaxy types displayed in Figure 1, including local and high-z galactic disks, starbursts at different redshifts, and even LSB galaxies, are described by a single relation with a slope consistent with 1.5, the one expected from Equation (3). The black curve in Figure 1 is the best fit to the sample of different galaxy populations (not including individual star-forming clouds), which corresponds to a slope of 1.43. Surprisingly, even individual star-forming clouds follow a similar trend, as expected from Equation (3), but shifted toward lower values of SFR per unit area. These results suggest that we are on the right track, but there is a fundamental difference in L between galaxies and star-forming clouds.

Is important to notice, aside from that the galactic radius R is not (a priori) a particularly meaningful scale in the star-formation problem, that the $R^{-1/2}$ term in Equation (3) is already able to erase the difference in star-formation efficiency between spirals and LSB galaxies, on which there has been considerable literature written (Bigiel et al. 2008, 2010; Wyder et al. 2009; Shi et al. 2011). Because LSBs are typically more extended than normal spirals, by almost a factor of 10 in the more extreme cases of Malin 1 or LSBC F568-06, the decrease due to the factor $R^{-1/2}$ explains their lower SFR per

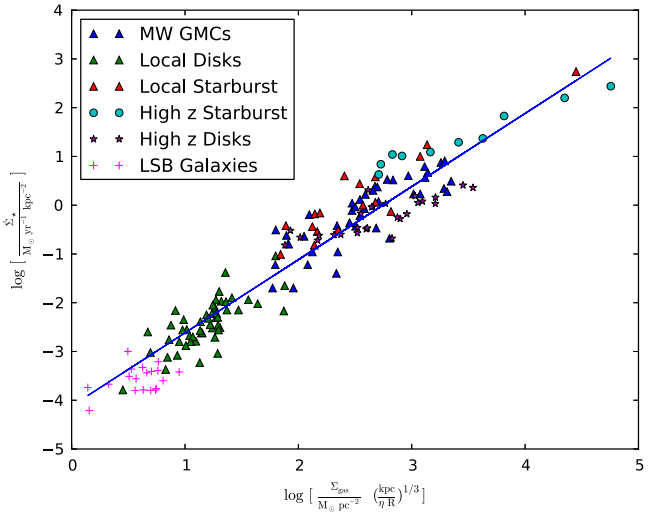

Figure 2. Same as Figure 1, but with the gas surface densities divided by the one-third power of the vertical scale length ($H = \eta R$). The blue line shows the fitting relation given in Equation (6), which has a scatter of 0.43 dex.

unit area for a fixed $\Sigma_{\rm gas}$. Therefore, a term that scales similar to R will be a good candidate for characteristic length L.

Star formation is inherently a three-dimensional (3D) problem, and the star-formation law is expressed in terms of some two-dimensional quantities: $\dot{\Sigma}_\star$ and $\Sigma_{\rm gas}$. The length-scale responsible for such a transition in dimensionality, an integration, is a natural candidate for being the characteristic length L. From an observational point of view, this integration scale will be in the observer's line of sight (LOS). In 3D numerical simulations, this will be the one chosen by the theorist, which is in most cases the vertical scale length. The difference between the cases is a projection factor, unless we are dealing with an edge-on disk, which we will neglect in this section and leave it in the scatter. Therefore, we will focus on estimations of the vertical scale length. We will come back to this point in Section 3.2

We will now estimate the characteristic length L to be equal to the vertical scale length, $H = \eta R$, and to avoid ad hoc fine-tuning, we will distinguish only between galaxy or region types. For typical disk galaxies, H/R is typically a few percent, so $\eta = 0.02$ is a good choice for LSB galaxies and normal spirals. Nuclear disks of starburst galaxies are more turbulent and thicker (Downes & Solomon 1998), and $\eta = 0.1$ will be our choice in this case. Similar cases are high-z disks and starbursts, again justifying the choice $\eta = 0.1$. Finally, because galactic GMCs are roughly spherical, in this case $\eta = 2$.

Figure 2 shows the SFR per unit area against $\Sigma_{\rm gas}(\eta R)^{-1/3}$, showing that, with this simple and more meaningful estimation for L, all of the star-forming regions, from local GMCs to high redshift galaxies, belong to a single relation of slope 1.5. The blue solid line corresponds to

$$\log \frac{\dot{\Sigma}_\star}{M_\odot\ {\rm kpc}^{-2}\ {\rm yr}^{-1}} = \frac{3}{2}\left(\log \frac{\Sigma_{\rm gas}}{M_\odot\ {\rm pc}^{-2}} - \frac{1}{3}\log \frac{\eta R}{\rm kpc}\right) - 4.1$$
$$= \frac{3}{2}\log \frac{\Sigma_{\rm gas}}{M_\odot\ {\rm pc}^{-2}} - \frac{1}{2}\log \frac{H}{\rm kpc} - 4.1, \qquad (6)$$

which has the same functional form as Equation (3) with $\log(\sqrt{G}\,\epsilon) = -4.1$ and has a scatter of 0.43 dex with respect to the data points. We have chosen to fit the data points with a fixed 3/2 slope, instead of using the best-fit one, which has a slope of 1.56 and a scatter of 0.429 dex, in order to preserve the correct dimensionality inferred from the Pi theorem. Deviations from the functional form with the correct dimensionality - should be associated with new physical parameters, like the ones introduced in Section 2.1 and Section 2.2, or with variations in intrinsic observational biases.

We found that, thanks to the $H^{-1/2}$ term from Equation (3), the data points in Figure 2 are consistent with a single star-formation law, with a scatter comparable to the one found by Daddi & Elbaz et al. (2010b) for $\dot{\Sigma}_\star \propto \Sigma_{\rm gas}/t_{\rm orb}$. However, the relation fitted by Daddi is not consistent with galactic GMCs (Krumholz et al. 2012), as it is for our Equation (3), which in addition is consistent with LSB galaxies. Also, Shi et al. (2011) previously brought the LSB galaxies to the spiral trend by introducing a $\Sigma_{\rm star}^{1/2}$ term, which for a stellar-dominated disk potential, with a given stellar velocity dispersion, is equivalent to an $H^{-1/2}$ term (van der Kruit 1988). It is important to emphasize that we choose η to be in agreement with the observed differences in thickness between the galaxies and star-forming regions displayed in Figure 2, and it is not an ad hoc extra, free parameter introduced to decrease the scatter in the relation.

The relatively higher scatter seen in individual star-forming regions should be expected because at those smaller scales other issues appear, such as time sampling in subgalactic regions, that are not included in Equation (3). For example, galaxies homogeneously sample the time line of star formation, whereas individual star-forming regions are at a specific point of such time line (Kruijssen & Longmore 2014). Formulations including Π_2 (Equation (4)), which can be expressed as the virial parameter, might take into account some of the differences in the evolutionary sequence: initial collapsing condensations (low $\alpha_{\rm virial}$), steady-state configurations ($\alpha_{\rm virial} \sim 1$), and the final evaporation ($\alpha_{\rm virial} \gg 1$) . However, for time sampling on even shorter timescales, new parameters should be added.

If the scatter in the relation for individual clouds is considerably reduced by including $\alpha_{\rm virial}$ or other physical parameters, we could expect those regions to depart from the same single relation of galactic systems. This is because the observed variables in star-formation laws are always averages at galactic scales, of quantities that vary strongly on the small length scales of individual clouds. Therefore, filling factors of gaseous clouds are very different compared to the averaged ones at galactic scales, and this has an effect on the normalization of the relation. In Section 3.2, we see an example of how the gas surface density and SFR are diluted by averaging over larger scales (kiloparsec).

The simplest possible interpretation for the relation shown in Figure 2 (Equation (6)) is in terms of the average free-fall time ($t_{\rm ff}$) at the characteristic length, which is now $H = \eta R$. Assuming a linear relation between total quantities, $\dot{M}_\star = \epsilon M_{\rm gas}/t_{\rm ff}$, dividing it by the total system area $A = R^2$, and noticing that $t_{\rm ff} = 1/\sqrt{G\rho} = 1/\sqrt{G\Sigma_{\rm gas}/H}$, it is straightforward to get $\dot{\Sigma}_\star = \epsilon\sqrt{G/H}\,\Sigma_{\rm gas}^{3/2}$. However, it is important to realize that the agreement between our dimensional analysis and the observed data is only telling us that such free-fall time is a characteristic timescale of the problem, but this doesn't mean that this simple picture, a monolithic free-fall collapse from the characteristic length, is how it happens in nature.

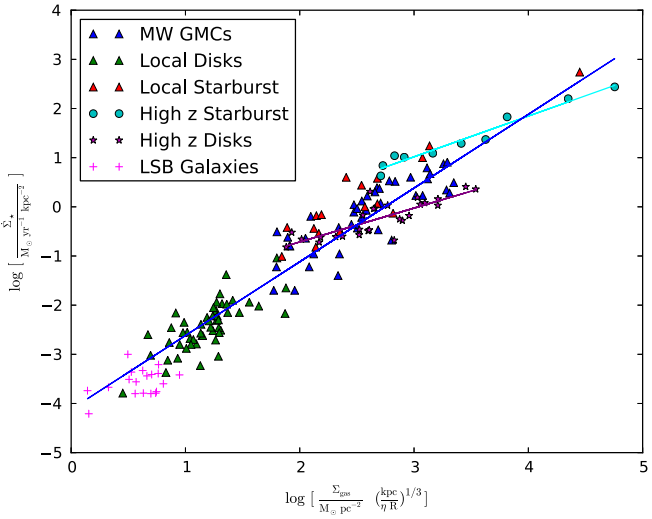

Figure 3. Same as Figure 2. The purple line shows a slope of ∼0.7 for the individual population of the high-z disks (Daddi et al. 2010a; Tacconi et al. 2010). The cyan line shows the slope (∼0.8) for the population of high-z starburst galaxies (Genzel et al. 2010).

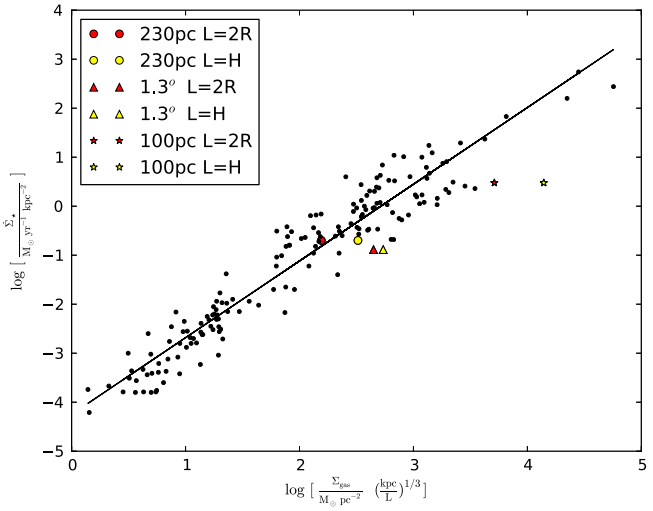

Figure 4. SFR density as a function of the gas surface density, divided by the one-third power of the integration scale length L. The yellow symbols indicate the location of the three CMZ regions, using L equal to the vertical thickness, and the red ones are the same regions but using L equal to the disk size. The black circles are the same galaxies and regions displayed in Figure 2.

The star-formation problem is controlled by nonlinear physics coming from gravity, turbulence, feedback from stars, and so on, which is far more complex than the simple free-fall interpretation in terms of averaged quantities. Only by performing detailed numerical experiments, which include the relevant physics, can light be shed on the exact reasons why this timescale is important. This is analogous to the case of Π_2, which we were able to find as a relevant parameter using dimensional analysis, but its exponential functional form and the reasons for it arise from numerical experiments.

Figure 2 also shows that the possible changes in slope in the KS law at lower surface densities (Bigiel et al. 2008; Wyder et al. 2009) are most probably due to variations of the integration scale L, instead of variations of the molecular gas fraction, as proposed by Bigiel et al. (2008). Moreover, Bigiel et al. (2010) found that the star-formation efficiency ($\Sigma_{\rm SFR}/\Sigma_{\rm gas}$) increases with $\Sigma_{\rm gas}$ (dominated by HI in their sample) and decreases with galactocentric radius R. In fact, Equation (3) and $L = H = \eta R$ imply a star-formation efficiency with the same trend, proportional to $\sqrt{\Sigma_{\rm gas}/R}$.

3.1. High-redshift Galaxies

The high redshift galaxies (filled circles and stars in Figure 2) as individual galaxy populations show slopes clearly departing from ∼3/2. This raises the question if new physical parameters are responsible for this change in slope, as was probably the case in the KS law at low surface densities (the extra $\sqrt{L}$ term).

Figure 3 shows the same data points as Figure 2, but with the individual slopes of the high-z disks (purple line) and starbursts (cyan line). Both populations have a slope considerably smaller, but surprisingly quite similar (∼0.7 for disks and ∼0.8 for starbursts). Because they are high-redshift systems, biases and resolution issues are always a possibility, but variations of other physical parameters might also produce noticeable changes in the efficiency ϵ.

In Section 4.1, we will explore the possibility of having the Toomre Q parameter (Toomre 1964) as a physical parameter controlling the efficiency ($\epsilon_{\rm SF} \propto e^{-Q}$). This allows us to interpret the weaker slope at high z as a sign of changes in the efficiency. One possible scenario is that the high-z galaxies richer in gas are undergoing a more extreme starburst episode, which generates enough energy to be in a state of larger Q, producing a significant decrease in the efficiency that compensates for their relatively higher surface densities.

3.2. The Central Molecular Zone

So far, we have not distinguished between L being the observer's LOS or the vertical thickness H, leaving the difference between both cases in the scatter. This difference is only a projection factor, square rooted, unless we are dealing with an edge-on system, in which case L should be related to the disk size. For that reason, a good starting point at which to study this effect is the central molecular zone (CMZ) because it is the nearest edge-on system and has an SFR lower than expected from the KS law (Kruijssen et al. 2014 and references therein).

In Figure 4 we study the location of three regions of the CMZ in the same star-formation plot shown in Figure 2 (displayed as filled black circles). The regions studied are the central 100 pc ring (stars), the 1.°3 complex (triangles), and the 230 pc zone (circles) that includes the two previous regions, with data taken from Kruijssen et al. (2014). The yellow symbols in Figure 4 indicate the location of the three CMZ regions, using L equal to the vertical thickness H, and the red ones are the same regions but using L equal to the disk size.

We find that in all cases that the red circles (L = disk size) are closer to the law given by Equation (6) (black line), as expected for a edge-on system like the CMZ. In the particular case of the central 100 pc ring, which was a clear outlier in the previous estimation (yellow star), the more meaningful choice for integration scale (L = disk size) is able to bring this region into the relation (within the scatter). This suggests that a systematic study is needed to quantify how much of the scatter seen in the relation is due to projection effects in the estimation of L, but this study is beyond the scope of this paper.

Finally, we wish to point out that the integrated 230 pc zone is clearly the closest to the relation given by Equation (6)

(black line). This is evidence that filling factors should play a role in the normalization of the law because its location is far from the average of the other two individual regions, suggesting that dilution is playing an important role. This region with size ∼0.5 kpc starts to be representative of the typical filling factors at galactic scales and reflects the differences from filling factors in "individual" star-forming regions or clouds and its effect on the relation.

Alternatively, if the differences between the integrated region and the two individual ones go beyond differences in filling factors, new physical parameters that affect the SF efficiency may explain the departures of the central 100 pc ring and the 1.°3 complex from the relation given by Equation (6) (black line), as we will discuss in the following section.

4. ON THE PHYSICS CONTROLLING THE CHARACTERISTIC LENGTH

The functional dependence found in Figure 2 (Equation (6)) relies on the integration scale L. For that reason, it is relevant to search for the galactic properties that determine such an integration scale. Discarding projection effects and avoiding edge-on systems, it is basically a question of what determines the vertical thickness of such a star-forming galaxy or region, and we will focus the discussion on such a case.

4.1. The Largest Scale Not Stabilized by Rotation

In disk galaxies, the vertical thickness is of the order of the largest scale not stabilized by rotation (Spitzer 1978), $\lambda_{\rm rot} \propto G\Sigma_{\rm gas}/\kappa^2$, where κ is the epicyclic frequency (see Binney & Tremaine 2008). The $\lambda_{\rm rot}$ length is the only scale intermediate between stars and galaxies that has a clear physical basis and determines the most massive clumps that are able to collapse (Escala & Larson 2008). This scale is also relevant for starburst galaxies because the bulk of the star formation comes from a massive nuclear disk (Downes & Solomon 1998). Moreover, even for systems without a large-scale ordered motion, like noncoplanar orbiting streams in a merger remnant, this scale can be generalized and is responsible for the width of individual star-forming streams (Escala et al. 2013). Therefore, the largest scale not stabilized by rotation is a natural candidate for controlling the characteristic integration length for galaxies.

Replacing L by $\lambda_{\rm rot}$ in Equation (3) and noticing that κ is aproximately equal to Ω, within a factor of two (Binney & Tremaine 2008), the star-formation law has the following expression:

$$\dot{\Sigma}_\star = \epsilon\ \Sigma_{\rm gas}\Omega = \epsilon\ \frac{\Sigma_{\rm gas}}{t_{\rm orb}}, \qquad (7)$$

which is one of the formulations studied in Kennicutt (1998) and is consistent with a single star-formation law for galaxies up to high z (Daddi & Elbaz et al. 2010b). For edge-on systems, the same scaling is expected, but with a different normalization, since rotational support implies $R \propto \sigma_{\rm gas}/\omega^2 f_{\rm gas}$, where $F_{\rm gas} = M_{\rm gas}/M_{\rm tot}$ is the gas mass fraction.

The second dimensionless parameter depends also on L, and when replaced by $\lambda_{\rm rot}$, it is $\Pi_2 = v_{\rm turb}\kappa/G\Sigma_{\rm gas}$, which is easily recognizable as the "turbulent" version of the Toomre parameter ($Q_{\rm turb}$; Toomre 1964). Under this scenario, to be in agreement with the exponential dependence of ϵ (Π_2) seen by Padoan et al. (2012), the star-formation law should be $\dot{\Sigma}_\star = \epsilon\ e^{-Q_{\rm turb}/q}\Sigma_{\rm gas}\Omega$, having q geometrical factors. The star-formation timescale, $\tau_{\rm SF} = \Sigma_{\rm gas}/\dot{\Sigma}_\star$, should also be proportional to $\exp(Q_{\rm turb}/q)t_{\rm orb}$. In fact, this exponential dependence in $\tau_{\rm SF}$ has been observed in numerical experiments of star formation in galactic disks, finding $\tau_{\rm SF} \propto \exp(Q_{\rm turb}/0.61)$ (Li et al. 2005). This numerical simulation does not find the $\tau_{\rm SF} \propto t_{\rm orb}$ dependence, simply because the orbital time is not varied between simulations (see their Table 1). Moreover, $\Pi_2(\lambda_{\rm rot})$ shows the equivalence between results in galactic-scale simulations (Li et al. 2005) and MHD simulations of GMCs (Padoan et al. 2012).

Finally, because it is observed that $Q_{\rm turb} \sim 1$ for most galaxies, this reconciles the apparent conflict between the strong exponential dependence on $Q_{\rm turb}$ and star-formation laws like KS, which aside from being independent of $Q_{\rm turb}$ are consistent with observations. Nevertheless, as discussed in the previous section, high-z galaxies as subpopulations tend to show a weaker slope than 3/2 (Figure 3). One possible scenario is that this weaker slope is a sign of changes in the efficiency ϵ due to significant variations of $Q_{\rm turb}$ in these extreme systems. For example, galaxies undergoing a extreme starburst episode that generates enough turbulence to be in a state of $Q_{\rm turb} > 1$ will produce a significant decrease of the efficiency ϵ.

4.2. The Turbulent Jeans Scale

Besides the several positive implications of identifying $\lambda_{\rm rot}$ as the characteristic length L, it is still worthwhile to explore alternatives. As discussed, from gravitational instability, it is clear that $\lambda_{\rm rot}$ (Escala & Larson 2008) is the characteristic length of collapsing clumps, and for unstable disks, such a scale is similar to the vertical thickness because this is when rotation starts to stabilize (and support) the system. However, it is more often found in the literature that the characteristic length of collapsing clumps is determined by the turbulent Jeans scale (e.g., Elmegreen 2002; Kim & Ostriker 2002). It is important to note that the condition $Q_{\rm turb} \sim 1$ is equivalent to having $\lambda_{\rm rot} \sim \lambda_{\rm jeans}$ (Escala & Larson 2008), and therefore it is hard to distinguish between the scales in most galaxies.

If we instead replace L by the two-dimensional "turbulent" Jeans scale, $\lambda_{\rm jeans} \propto v_{\rm turb}^2/G\Sigma_{\rm gas}$, Equation (3) can be rewritten as $\dot{\Sigma}_\star = \epsilon G\Sigma_{\rm gas}^2 v_{\rm turb}^{-1}$. This is the same star-formation law found in a scenario where turbulence from a starburst regulates the vertical height (Equation (21) in Ostriker & Shetty 2011). The second dimensionless parameter in such a case, $\Pi_2 = v_{\rm turb}\left(G\Sigma_{\rm gas}\lambda_{\rm jeans}\right)^{-1/2}$, is equal to one, meaning that $Q_{\rm turb}$ becomes irrelevant and that this scenario is only valid in the particular case of $Q_{\rm turb} \sim 1$. This also supports the scenario in which the vertical height is controlled by the large-scale galactic potential ($\lambda_{\rm rot}$) and is the self-regulation loop of Goldreich & Lynden-Bell (1965), which pushes $\lambda_{\rm jeans}$ toward $\lambda_{\rm rot}$ ($Q_{\rm turb} \sim 1$), as discussed in Escala (2011).

4.3. Individual Star-forming Clouds

For individual star-forming clouds with sizes smaller than the galactic vertical thickness, their characteristic length L is their diameter $2R$. In order to include the possibility of out-of-equilibrium configurations, as in Section 4.1, it is convenient to express it in terms of the virial parameter $\alpha_{\rm virial} \equiv 2\,T/W$.

Within geometrical factors, the virial parameter is on the order of $Rv_{\rm turb}^2/GM_{\rm c}$, being $M_{\rm c}=\Sigma_{\rm gas}R^2$, the cloud's total gas mass, or equivalently, $R=v_{\rm turb}^2/G\Sigma_{\rm gas}\alpha_{\rm virial}$.

Identifiying R as the characteristic length in the second dimensionless parameter, it becomes $\Pi_2=\alpha_{\rm virial}$. Motivated by the fitted star-formation efficiency $\epsilon_{\rm ff}\propto \exp\left(-1.74v_{\rm turb}\left(G\Sigma_{\rm gas}L\right)^{-1/2}\right)$ of Padoan et al. (2012), for individual clouds Equation (5) can be rewritten as

$$\dot{\Sigma}_\star=\epsilon\left[\mathcal{M}_{\rm s},\,\mathcal{M}_a\right]\sqrt{\frac{G}{2R}}\,\Sigma_{\rm gas}^{3/2}\,e^{-1.23\alpha_{\rm virial}}. \quad (8)$$

5. DISCUSSION

In this paper, we have explored an alternative approach to studying the universal star-formation law. Instead of using idealized analytical models to study this inherently complex and multiparametric problem, like most in modern astronomy, we used the Pi theorem of dimensional analysis to search for the relevant physical variables. In addition, this approach avoids the temptation of overinterpreting simple "spherical cow" models.

Using the Vaschy–Buckingham Pi theorem, we find that the star-formation law should have a form $\dot{\Sigma}_\star=\epsilon\sqrt{\frac{G}{L}}\Sigma_{\rm gas}^{3/2}$, where L is a characteristic length. We argued that L should be related to the integration scale, which transforms relevant 3D quantities in the star-formation problem into 2D ones, like $\dot{\Sigma}_\star$ and $\Sigma_{\rm gas}$. Using simple estimations for L, we find that galaxies of different types and redshifts, including LSB Galaxies and individual star-forming regions in our Galaxy, obey this single star-formation law.

The only free parameter introduced in our analysis is η, in $L=H=\eta R$, which is in principle a possible caveat of the present analysis. However, we choose observed values that vary from 0.02 for spirals or LSB galaxies to 2 for individual clouds, a range at most a factor of 10 in $\sqrt{\eta}$. For local starbursts and high-z disks, we choose a larger value of 0.1, which is in agreement with the measured values in starbursts (Downes & Solomon 1998) and with the larger thickness predicted (Kroupa 2002) and estimated (Elmegreen & Elmegreen 2005) for gas-rich, high-z disks. The only debatable value is the choice of $\eta=0.1$ for high-z starbursts (Genzel et al. 2010). However, a choice of $\eta=0.4$ will only increase the scatter in Figure 2 to 0.45 dex and $\eta=1$ to 0.47 dex. We decide to not vary the parameter η at this level because these are variations comparable to other possible sources of error, such as the CO conversion factors assumed in Genzel et al. (2010).

We also find that, depending on the assumption chosen for the vertical scale length H, this star-formation law adopts the different formulations previously studied in the literature. For a constant H, we recover the standard KS law. For $H=\lambda_{\rm rot}$, we recover $\dot{\Sigma}_\star\propto\Sigma_{\rm gas}/t_{\rm orb}$, and for $H=\lambda_{\rm Jeans}$, we find $\dot{\Sigma}_\star\propto\Sigma_{\rm gas}^2/v_{\rm turb}$.

As a vertical scale length, we favor $H=\lambda_{\rm rot}$ because this is the characteristic length of the most massive collapsing clumps, and for unstable disks, such a scale is comparable to the vertical thickness, because this is when rotation starts to stabilize and globally support the system. In such a case, Π_2 can be identified as the Toomre parameter $Q_{\rm turb}$, allowing us to include systems out of equilibrium ($Q_{\rm turb}\neq 1$). This case suggests that for galaxies a universal star-formation law has the form

$$\dot{\Sigma}_\star=\epsilon\left[\mathcal{M}_{\rm s},\,\mathcal{M}_a\right]e^{-\frac{Q_{\rm turb}}{q}}\sqrt{\frac{G}{\lambda_{\rm rot}}}\,\Sigma_{\rm gas}^{3/2}, \quad (9)$$

which is expressed in terms of physical variables related to local and global properties. Using $\lambda_{\rm rot}\propto G\Sigma_{\rm gas}/\kappa^2$, this equation is equivalent to

$$\dot{\Sigma}_\star=\epsilon\left[\mathcal{M}_{\rm s},\,\mathcal{M}_a\right]e^{-\frac{Q_{\rm turb}}{q}}\Sigma_{\rm gas}\,\kappa, \quad (10)$$

where κ is approximately equal to Ω, within factors of two. This can be generalized to systems without large-scale ordered motion (mergers), by replacing κ by the modulus of the orbital frequency vector Ω_0 (Escala et al. 2013), which also depends on the center of rotation 0. The exponential decay on the efficiency in Equation (10) is so far only supported by numerical experiments, so it would be interesting to test such dependence with observations, more specifically if this can take into account part of the observed scatter in the star-formation law.

In summary, we have shown the advantages of using the Vaschy–Buckingham Pi theorem to guide the analysis of the results coming from numerical simulations and observations. Future observations of star formation under more extreme environments, complemented with new numerical experiments that include more physics and a larger dynamical range, could shed light in finding new physical variables and their functional dependence in the star-formation law.

I thank D. Kruijssen, A. Guzman, F. Becerra, P. Coppi, R. Larson, and the anonymous referee for very valuable comments. A.E. acknowledges partial support from the Center for Astrophysics and Associated Technologies CATA (PFB Q6), Anillo de Ciencia y Tecnologia (Project ACT1101), and Proyecto Regular Fondecyt (grant 1130458).

REFERENCES

Ballesteros-Paredes, J., Klessen, R. S., Mac Low, M.-M., & Vazquez-Semadeni, E. 2007, Protostars and Planets V (Tucson: Univ. Arizona Press)
Becerra, F., & Escala, A. 2014, ApJ, 786, 56
Bigiel, F., Leroy, A., Walter, F., et al. 2008, AJ, 136, 2846
Bigiel, F., Leroy, A., Walter, F., et al. 2010, AJ, 140, 1194
Binney, J., & Tremaine, S. 2008, Galactic Dynamics (Princeton: Princeton Univ. Press)
Bonnor, W. B. 1956, MNRAS, 116, 351
Daddi, E., Bournaud, F., Walter, F., et al. 2010a, ApJ, 713, 686
Daddi, E., Elbaz, D., Walter, F., et al. 2010b, ApJL, 714, L118
Dib, S., Piau, L., Mohanty, S., & Braine, J. 2011, MNRAS, 415, 3439
Downes, D., & Solomon, P. M. 1998, ApJ, 507, 615
Ebert, R. 1955, ZA, 37, 217
Elmegreen, B. G., & Elmegreen, D. M. 2005, ApJ, 627, 632
Elmegreen, B. G. 2002, ApJ, 577, 206
Escala, A., & Larson, R. B. 2008, ApJL, 685, L31
Escala, A. 2011, ApJ, 735, 56
Escala, A., Becerra, F., del Valle, L., & Castillo, E. 2013, ApJ, 763, 39
Federrath, C. 2013, MNRAS, 436, 3167
Genzel, R., Tacconi, L. J., Gracia-Carpio, J., et al. 2010, MNRAS, 407, 2091
Goldreich, P., & Lynden-Bell, D. 1965, MNRAS, 130, 125
Guillard, P., Boulanger, F., Lehnertet, M. D., et al. 2014, arXiv:1410.6155
Heiderman, A., Evans, N. J., II, Allen, L. E., Huard, T., & Heyer, M. 2010, ApJ, 723, 1019
Hodge, P. A., Riechers, D., Decarli, R., et al. 2015, ApJ, 798, 18
Hopkins, P. 2013, MNRAS, 430, 1653

Jeans, J. H. 1902, RSPTA, 199, 1
Kenney, J. D. P., Wilson, C. D., Scoville, N. Z., Devereux, N. A., & Young, J. S. 1992, ApJL, 395, L79
Kennicutt, R. C. 1998, ApJ, 498, 541
Kim, W., & Ostriker, E. C. 2002, ApJ, 570, 132
Kroupa, P. 2002, MNRAS, 330, 707
Kruijssen, J. M. D., & Longmore, S. N. 2014, MNRAS, 439, 3239
Kruijssen, J. M. D., Longmore, S. N., Elmegreen, B. G., et al. 2014, MNRAS, 440, 3370
Krumholz, M. R., & McKee, C. F. 2005, ApJ, 630, 250
Krumholz, M. R., Dekel, A., & McKee, C. F. 2012, ApJ, 745, 69
Lada, C. J., Lombardi, M., & Alves, J. F. 2010, ApJ, 724, 687
Larson, R. B. 1969, MNRAS, 145, 271
Larson, R. B. 1979, MNRAS, 186, 479
Larson, R. B. 1981, MNRAS, 194, 809
Leroy, A. K., Walter, F., Brinks, E., et al. 2008, AJ, 136, 2782
Li, Y., Mac Low, M.-M., & Klessen, R. S. 2005, ApJ, 626, 823
Mac Low, M.-M., & Klessen, R. S. 2004, RvMP, 76, 125
Mouschovias, T. C. 1974, ApJ, 192, 37
Ostriker, E. C., & Shetty, R. 2011, ApJ, 731, 41
Padoan, P., Haugbolle, T., & Nordlund, A. 2012, ApJL, 759, L27
Padoan, P., & Nordlund, A. 2011, ApJ, 730, 40
Penston, M. V. 1969, MNRAS, 144, 425
Schmidt 1959, ApJ, 129, 243S
Shi, Y., Armus, L., Helou, G., et al. 2014, Natur, 514, 335
Shi, Y., Helou, G., Yan, L., et al. 2011, ApJ, 733, 87
Silk, J. 1997, ApJ, 481, 703
Shu, F. H. 1997, ApJ, 214, 488
Smith, B. J., & Harvey, P. M. 1996, ApJ, 468, 139
Spitzer, L. 1978, Physical Processes in the Interstellar Medium (New York: Interscience)
Stinson, G., Seth, A., Katz, N., et al. 2006, MNRAS, 373, 1074
Tacconi, L. J., Genzel, R., Neri, R., et al. 2010, Natur, 463, 781
Tasker, E., & Bryan, G. L. 2006, ApJ, 641, 878
Tasker, E., & Tan, J. 2009, ApJ, 700, 358
Toomre, A. 1964, ApJ, 139, 1217
Telesco, C. M., Dressel, L. L., & Wolstencroft, R. D. 1993, ApJ, 414, 120
van der Kruit, P. C. 1988, A&A, 192, 117
Wild, W., Harris, A. I., Eckart, A., Genzel, R., et al. 1992, A&A, 265, 447
Wyder, T., Martin, D. C., Barlow, T. A., et al. 2009, ApJ, 696, 1834
Xu, C. K., Cao, C., Lu, N., et al. 2014, arXiv:1411.1111
Young, J., Xie, S., Tacconi, L., et al. 1995, ApJSS, 98, 219